Investigation of the Environment Surrounding Iron−Sulfur Cluster 4 of *Escherichia coli* Dimethylsulfoxide Reductase†

Victor W. T. Cheng,‡ Richard A. Rothery,‡ Michela G. Bertero,§ Natalie C. J. Strynadka,§ and Joel H. Weiner*,‡

Membrane Protein Research Group, Department of Biochemistry, University of Alberta, 474 Medical Sciences Building, Edmonton, Alberta T6G 2H7, Canada, and Department of Biochemistry, University of British Columbia, 2146 Health Sciences Mall, Vancouver, British Columbia V6T 1Z3, Canada

Received February 25, 2005; Revised Manuscript Received April 12, 2005

ABSTRACT: Iron−sulfur ([Fe-S]) clusters are common in electron transfer proteins, and their midpoint potentials (E_m values) play a major role in defining the rate at which electrons are shuttled. The E_m values of [Fe-S] clusters are largely dependent on the protein environment as well as solvent accessibility. The electron transfer subunit (DmsB) of *Escherichia coli* dimethylsulfoxide reductase contains four [4Fe-4S] clusters (FS1−FS4) with E_m values between −50 and −330 mV. We have constructed an *in silico* model of DmsB and addressed the roles of a group of residues surrounding FS4 in electron transfer, menaquinol (MQH_2) binding, and protein control of its E_m. Residues Pro80, Ser81, Cys102, and Tyr104 of DmsB are located at the DmsB−DmsC interface and are critical for the binding of the MQH_2 inhibitor analogue 2-*n*-heptyl-4-hydroxyquinoline *N*-oxide (HOQNO) and the transfer of electrons from MQH_2 to FS4. Because the EPR spectrum of FS4 is complicated by spectral overlap and spin−spin interactions with the other [4Fe-4S] clusters of DmsB, we evaluated mutant effects on FS4 in double mutants (with a DmsB-C102S mutation) in which FS4 is assembled as a [3Fe-4S] cluster ($FS4^{[3Fe-4S]}$). The DmsB-C102S/Y104D and DmsB-C102S/Y104E mutants dramatically lower the E_m of $FS4^{[3Fe-4S]}$ from 275 to 150 mV and from 275 to 145 mV, respectively. Mutations of positively charged residues around $FS4^{[3Fe-4S]}$ lower its E_m, but mutations of negatively charged residues have negligible effects. The E_m of $FS4^{[3Fe-4S]}$ in the DmsB-C102S mutant is insensitive to HOQNO as well as to changes in pH from 5 to 7. The $FS4^{[3Fe-4S]}$ E_m of the DmsB-C102S/Y104D mutant increases in the presence of HOQNO and decreasing pH. Analyses of the mutants suggest that the maximum achievable E_m for $FS4^{[3Fe-4S]}$ of DmsB is approximately 275 mV.

The bacterium *Escherichia coli* can grow anaerobically on dimethyl sulfoxide (Me_2SO)[1] as a terminal electron acceptor by expressing a respiratory chain that begins with a suitable dehydrogenase, terminates with a menaquinol: Me_2SO oxidoreductase (DmsABC), and uses menaquinol (MQH_2) to shuttle electrons between both enzymes (*1*, *2*). The *dmsABC* operon has been cloned and sequenced (*3*), and the enzyme can be expressed and assembled to high levels in the cytoplasmic membrane (*4*). DmsABC has broad substrate specificity with respect to a variety of *S*- and *N*-oxides, including Me_2SO and trimethylamine *N*-oxide (Me_3NO) (*5*).

DmsABC is a heterotrimeric molybdoenzyme that comprises two membrane extrinsic subunits (DmsA and DmsB) that are anchored to the cytoplasmic membrane by the integral membrane subunit (DmsC) (*6*). DmsA and DmsB comprise a catalytic dimer that is targeted to the cytoplasmic membrane by the Sec-independent Mtt/Tat translocon (*7*). DmsA (85.8 kDa) is the catalytic subunit which contains a molybdo-bis(molybdopterin guanine dinucleotide) cofactor (Mo-bisMGD) at its active site, where Me_2SO is reduced to dimethyl sulfide (*8*). DmsB (22.7 kDa) is the electron transfer subunit which contains four [4Fe-4S] clusters, FS1−FS4 (*9*). DmsC (30.8 kDa) comprises eight transmembrane helices (*10*), and is essential for MQH_2 binding and oxidation (*11*−*13*).

DmsABC is an archetype of an important family of bacterial [Fe-S]-molybdoenzymes that includes the *E. coli* formate dehydrogenases (FdnGHI and FdoGHI) (*14*−*16*), the *E. coli* membrane-bound nitrate reductases (NarGHI and NarZYV) (*17*−*19*), *Salmonella typhimurium* thiosulfate reductase (PhsABC) (*20*), and *Wolinella succinogenes* polysulfide reductase (PsrABC) (*21*, *22*). Each member of this family has a catalytic subunit containing a molybdenum

† This work was funded by the Canadian Institutes of Health Research. Infrastructure funding was provided by the Canada Foundation for Innovation. V.W.T.C. was supported by an Alberta Heritage Foundation for Medical Research Graduate Studentship. J.H.W. holds a Canada Research Chair in Membrane Biochemistry.

* To whom correspondence should be addressed. Telephone: (780) 492-2761. Fax: (780) 492-0886. E-mail: joel.weiner@ualberta.ca.

‡ University of Alberta.

§ University of British Columbia.

[1] Abbreviations: $BV^{+\bullet}$, reduced benzyl viologen; DmsABC, *E. coli* Me_2SO reductase; E_m, midpoint potential; FCP, four-cluster protein; FQ, fluorescence quench; FdnGHI, *E. coli* formate dehydrogenase-N; FrdABCD, *E. coli* fumarate reductase; HOQNO, 2-*n*-heptyl-4-hydroxyquinoline *N*-oxide; $LPCH_2$, reduced lapachol [2-hydroxy-3-(3-methyl-2-butenyl)-1,4-naphthoquinone]; Me_2SO, dimethyl sulfoxide; Me_3NO, trimethylamine *N*-oxide; Mo-bisMGD, molybdo-bis(molybdopterin guanine dinucleotide); MQH_2, menaquinol; NarGHI, *E. coli* nitrate reductase A; Q-site, quinol-binding site; rmsd, root-mean-square deviation; SdhCDAB, *E. coli* succinate dehydrogenase; UQ, ubiquinone.

10.1021/bi050362p CCC: $30.25
Published on Web 05/12/2005

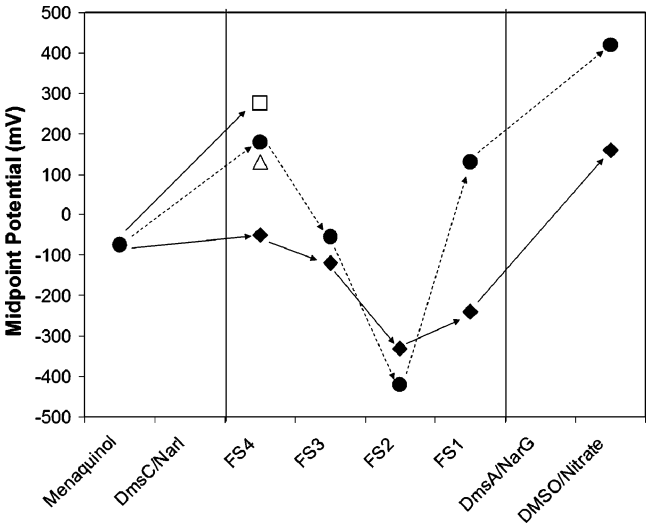

FIGURE 1: Electron transfer through DmsB (◆) and NarH (●). The E_m values of each [Fe-S] cluster in both electron transfer subunits are shown. FS4 of the DmsB-C102S mutant (△) and FS4 of the DmsB-C102S/Y104D/H106F mutant (□) are also shown. Both the DmsB-C102S mutant and the DmsB-C102S/Y104D/H106F mutant are nonfunctional. Note that the $E_{m,7}$ for the FS4−FS2 pair is −600 mV in NarH, −280 mV in DmsB, −460 mV in the DmsB-C102S/Y104D/H106F mutant, and −605 mV in the DmsB-C102S mutant.

cofactor in the form of Mo-bisMGD and a [4Fe-4S] cluster (FS0) (*14*, *17*), an electron transfer subunit containing four [Fe-S] clusters (four-cluster protein, FCP), and a hydrophobic membrane anchor subunit. The various prosthetic groups of these enzymes catalyze overall reactions that transfer two electrons through the FCP to or from a quinol-binding site (Q-site) that is associated with the membrane anchor domain (*18*).

DmsB is highly homologous with FdnH and NarH, both of which are FCP subunits of membrane-bound heterotrimeric redox enzymes that recently have had their X-ray crystallographic structures elucidated to high resolution (*14*, *17*). The four [Fe-S] clusters of these subunits are arranged in an almost linear fashion that facilitates electron shuttling between the active site and the Q-site, and are called FS1 (closest to the catalytic subunit), FS2, FS3, and FS4 (closest to the Q-site). The four [4Fe-4S] clusters in DmsB have midpoint potentials (E_m values) of −50 (FS4), −120 (FS3), −330 (FS2), and −240 mV (FS1) (*9*, *12*). NarH contains three [4Fe-4S] clusters and one [3Fe-4S] cluster, with E_m values of 180 (FS4, [3Fe-4S] cluster), −50 (FS3), −420 (FS2), and 130 mV (FS1) (*19*, *23*, *24*). Thus, the profiles of the E_m values are quite similar for DmsB and NarH (Figure 1). The E_m values for the [4Fe-4S] clusters of FdnH have yet to be determined.

In addition to DmsABC and NarGHI, a number of *E. coli* respiratory chain enzymes containing [Fe-S] clusters have been examined in detail by redox potentiometry, including MQH_2:fumarate oxidoreductase (FrdABCD) (*25*, *26*) and succinate:UQ oxidoreductase (SdhCDAB) (*27*). Two aspects of the redox potentiometry of [Fe-S] clusters are under intense study: (i) the role of the E_m value in defining the rates of electron transfer through a string of clusters (*28*−*30*) and (ii) the role of the coordination environment in defining the E_m value (*31*, *32*). A number of factors have been proposed to control [Fe-S] cluster E_m, including (i) the local hydrogen bonding network, (ii) the local electrostatic field, (iii) solvent accessibility, and (iv) backbone amides (*31*−*37*). DmsABC is a model enzyme in which we can evaluate factors that may modulate [Fe-S] cluster E_m values and intercenter electron transfer rates.

One fundamental difference between FdnGHI/NarGHI and DmsABC is the presence of *b*-type hemes in the transmembrane subunits of the former enzymes and the absence of heme in the latter enzyme. Thus, in DmsABC, there is a direct transfer of electrons from MQH_2 to FS4 (*4*) in a manner similar to the transfer of electrons from the Q_p site to the [3Fe-4S] cluster of FrdABCD (*38*−*40*). In the structure of FdnH, the side chain of a conserved Tyr residue is pointing toward the FdnI subunit and interacts with the proximal heme. Since DmsABC does not contain heme, we hypothesize that the equivalent residue in DmsB (Tyr104) may play an important role in MQH_2 binding and oxidation, and may be critical in directing electrons from MQH_2 to FS4. A related question arises regarding the role of heme(s) in the family of FrdABCD/SdhCDAB enzymes in different organisms, wherein zero, one, or two hemes may be present in the membrane anchor domain (*40*, *41*).

In this study, we have investigated the role of the protein environment in influencing the redox properties of the FS4 cluster of DmsB by using a combination of site-directed mutagenesis, redox potentiometry, and EPR spectroscopy. To eliminate spectral complications arising from spin−spin interactions between multiple reduced [4Fe-4S] clusters of DmsB, we have evaluated the effects of point mutations in a DmsB-C102S mutant that contains a high-potential [3Fe-4S] FS4 cluster ($FS4^{[3Fe-4S]}$) that is magnetically isolated in its oxidized form. We have also evaluated the effects of the mutants on MQH_2 binding and on the kinetics of the enzyme containing the native [4Fe-4S] cluster form of FS4 ($FS4^{[4Fe-4S]}$). These studies will aid in improving our understanding of the factors controlling the E_m of [Fe-S] clusters and their effects on the electron transfer rate.

EXPERIMENTAL PROCEDURES

Homology Modeling. Sequence identity searches were conducted with BLAST (*42*). Threading calculations were performed with MODELLER version 6.0a (*43*) using the *E. coli* FdnH structure as the template (PDB entry 1KQF). The quality of the DmsB model was validated with PROCHECK (*44*). The model that was generated represents 84.6% of the residues in most favorable regions, 13.3% in additional allowed regions, and 2.1% in generously allowed regions.

Bacterial Strains and Plasmids. The *E. coli* strains used in this study include HB101 [*supE*44 *hsdS*20 (r_B-m_B-) *recA*13 *ara*-14 *proA*2 *lacY*1 *galK*2 *rpsL*20 *xyl*-5 *mtl*-1 (lab collection)], TG1 [*supE hsd*Δ5 *thi* Δ(*lac-proAB*) *F′*[*traD*36 *proAB*$^+$ *lacI*^{q} *lacZ*ΔM15] (Amersham Biosciences)], DSS301 [TG1, Δ*dmsABC* (lab collection) (*11*)], and TOPP2 [*rif*^{R} *[F′, proAB, lacI*^{q}ZΔ*M15*, Tn*10*,(*tet*^{r})*]* (Stratagene)]. The plasmids used for cloning and expression include pBR322 [$Tet^R Amp^R$ (Pharmacia)], pTZ18R [Amp^R*lacZ′* (Pharmacia)], pDms160 [*dmsABC* cloned into the EcoRI−SalI fragment of pBR322 (lab collection) (*4*)], pDms170 [pDms160 derivative (lab collection) (*45*)], pBTZ [EcoRI−SacI fragment of pDms160 cloned into pTZ18R (this study)], and pBTZ1021 [EcoRI−SacI fragment of pDms160-DmsB-C102S (*4*) cloned into pTZ18R (this study)].

Cloning. Mutagenic oligonucleotides were designed with the addition and/or deletion of restriction sites in the DNA sequence to facilitate the screening process, and were purchased from Sigma Canada. Mutants were generated using the QuickChange site-directed mutagenesis kit from Stratagene, with the pBTZ and pBTZ1021 plasmids as templates for the QuickChange reactions. DpnI was purchased from Invitrogen, and DNA purification kits were purchased from Qiagen. Mutants were verified by DNA sequencing (DNA Core Facility, Department of Biochemistry, University of Alberta) and cloned back into the pDms160 expression vector. The mutant plasmids were then transformed into both *E. coli* HB101 and DSS301 for biochemical studies. Preparation of competent cells and transformations of plasmids into competent cells were carried out as described in *Molecular Cloning: A Laboratory Manual* (*46*).

Growth of Bacteria. Variants of the pDms160 expression plasmid containing the desired DmsB mutations were transformed into DSS301 cells. The ability of the mutant enzymes to support respiratory growth in Me_2SO was evaluated by growing the cells anaerobically at 37 °C in glycerol/Me_2SO minimal medium and monitoring cell turbidity using a Klett-Summerson spectrophotometer equipped with a no. 66 filter as previously described (*1*). For the preparation of membranes, HB101 cells were allowed to grow anaerobically for 48 h in 19 L of glycerol/fumarate medium, whereas DSS301 cells were grown for 24 h in 1 L of glycerol/fumarate medium (*4*).

Preparation of Membranes. Membranes were prepared by French pressure cell lysis and differential centrifugation as previously described (*9*). Essentially, cells were pelleted, washed, and resuspended in 50 mM MOPS/5 mM EDTA buffer (pH 7). Cells were French pressed after addition of dithiothreitol and phenylmethanesulfonyl fluoride (PMSF) to final concentrations of 1 and 0.2 mM, respectively. Membranes were washed and pelleted by centrifugation in a Beckman 50.2Ti rotor at 150000*g* for 90 min, then homogenized in 50 mM MOPS/5 mM EDTA buffer (or 100 mM MOPS/5 mM EDTA buffer for EPR samples), and flash-frozen with liquid N_2. Protein concentrations were determined with a modified Lowry assay containing 1% (w/v) SDS (*47*).

Enzyme Assays. The benzyl viologen ($BV^{+\bullet}$)-dependent reduction of trimethylamine *N*-oxide (Me_3NO) has been described previously (*9*). The extinction coefficient of $BV^{+\bullet}$ is 7.4 $mmol^{-1}$ cm^{-1}, measured at its absorbance maximum of 570 nm. The lapachol ($LPCH_2$)-dependent anaerobic reduction of Me_3NO has also been described previously (*48*). The extinction coefficient for $LPCH_2$ is 2.66 $mmol^{-1}$ cm^{-1}, measured at a wavelength of 481 nm.

HOQNO Fluorescence Quench (FQ) Titrations. 2-*n*-Heptyl-4-hydroxyquinoline *N*-oxide (HOQNO) binding was monitored by fluorescence according to the method of van Ark and Berden (*49*). Aliquots (2 μL) of 0.1 mM HOQNO were added to the sample, and fluorescence was measured at an excitation wavelength of 341 nm and an emission wavelength of 479 nm. The experiment was carried out at protein concentrations of 0.25, 0.50, and 0.75 mg/mL. The concentration of HOQNO binding sites and the dissociation constant of HOQNO were estimated by fitting the data as described by Okun et al. (*50*) using the equation

$$F_{obs} = (f_{bound} - f_{free})[Q - (Q^2 - n_s[E_{tot}][I_{tot}])^{1/2}] + f_{free}[I_{tot}]$$

with

$$Q = 0.5([I_{tot}] + K_d + n_s[E_{tot}]) \text{ and } [I_{tot}] = [I_{bound}] + [I_{free}]$$

The terms f_{bound} and f_{free} refer to the fluorescence of bound and free HOQNO, respectively (f_{bound} is zero for HOQNO). $[I_{tot}]$, $[I_{bound}]$, and $[I_{free}]$ are the concentrations of total, bound, and free HOQNO, respectively. $[E_{tot}]$ is the total concentration of the enzyme (given as nanomoles of DmsABC per milligram of total protein in Table 2), and n_s is the number of inhibitor binding sites (for DmsABC, $n_s = 1$) (*51*).

EPR Spectroscopy. Membrane vesicles were prepared in 100 mM MOPS/5 mM EDTA (pH 7) buffer with a final protein concentration of approximately 30 mg/mL. Membranes were prepared in 100 mM MES/5 mM EDTA (pH 6) and 100 mM acetate/5 mM EDTA (pH 5) buffers for pH studies. Redox titrations were carried out at 25 °C under argon in an anaerobic chamber as previously described (*12*, *24*), and the following redox dyes were added to a final concentration of 50 μM: quinhydrone ($E_{m,7} = 286$ mV), 2,6-dichloroindophenol ($E_{m,7} = 217$ mV), 1,2-naphthoquinone ($E_{m,7} = 125$ mV), toluylene blue ($E_{m,7} = 115$ mV), phenazine methosulfate ($E_{m,7} = 80$ mV), thionine ($E_{m,7} = 60$ mV), duroquinone ($E_{m,7} = 7$ mV), methylene blue ($E_{m,7} = -11$ mV), resorufin ($E_{m,7} = -50$ mV), indigo trisulfonate ($E_{m,7} = -80$ mV), indigo disulfonate ($E_{m,7} = -125$ mV), anthraquinone-2-sulfonic acid ($E_{m,7} = -225$ mV), phenosafranine ($E_{m,7} = -255$ mV), benzyl viologen ($E_{m,7} = -360$ mV), and methyl viologen ($E_{m,7} = -440$ mV). All samples were prepared in 3 mm internal diameter quartz EPR tubes and were rapidly frozen in liquid nitrogen-chilled ethanol before being stored in liquid nitrogen. EPR spectra were recorded using a Bruker Elexsys E500 EPR spectrometer equipped with an Oxford Instruments ESR900 flowing helium cryostat. Instrument conditions and temperatures were described in the individual figure legends, and spectra were corrected for tube calibration. EPR studies were only carried out on enzymes which have both the desired mutation in DmsB and the DmsB-C102S mutation so that a magnetically isolated oxidized [3Fe-4S] signal can be observed.

RESULTS

Selection of Residues for Mutagenesis. Both *E. coli* FdnH and DmsB contain four [Fe-S] clusters which are coordinated by four ferredoxin-like Cys motifs (*52*). Alignment of DmsB with FdnH reveals 37% sequence identity between the two proteins. A significant difference between the two is that FdnH has a transmembrane C-terminal tail (*14*) whereas DmsB is predicted to be entirely membrane-extrinsic (*11*). A ClustalW alignment of the local amino acids from FdnH and DmsB immediately surrounding FS4 shows significant sequence similarity and inferred structural similarity (Figure 2). To aid in the selection of targets for mutagenesis and subsequent analysis, a structural model of DmsB was generated with MODELLER version 6.0 (*43*) using the FdnH 1.6 Å resolution X-ray crystal structure as the template. The amino acid residues in DmsB which were subjected to site-directed mutagenesis studies are depicted in Figures 2 and 3. These were chosen on the basis of their proximity (<10 Å) to FS4 in the FdnH structure and in the DmsB model. A variety of charged, apolar, and aromatic residues were selected for site-directed mutagenesis studies. Figure 4 shows

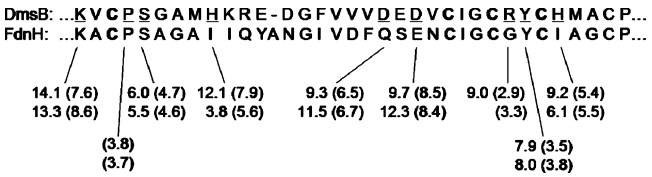

FIGURE 2: Local alignment of the amino acids around FS4 of DmsB with that of FdnH. The four cysteines in bold are ligands to $FS4^{[4Fe-4S]}$. Underlined residues indicate the positions at which DmsB mutants were generated. Indicated are the distances from the DmsB (top) and FdnH (bottom) amino acid side chains (and backbone amides) to FS4 in angstroms.

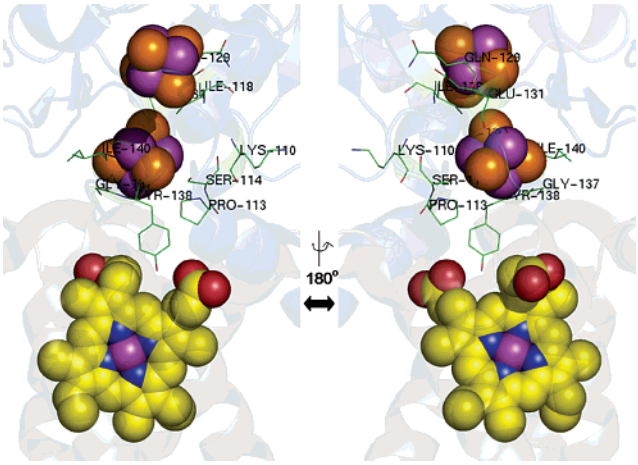

FIGURE 3: Crystal structure of FdnGHI, magnified and centered on FS4. Highlighted are the equivalent residues in FdnH which were studied by site-directed mutagenesis in DmsB. The proximal heme of FdnI is also shown. Note that the proline, serine, and tyrosine residues are all located at the interface between the FdnH electron transfer subunit and the FdnI membrane anchor subunit, and that the latter residue plays a critical role by interacting with the proximal heme of FdnI. Pro113, Ser114, and Tyr138 of FdnH are equivalent to Pro80, Ser81, and Tyr104 of DmsB, respectively.

an overlay of the DmsB model with the FdnH structure. The DmsB model superimposes onto the FdnH structure with a root-mean-square deviation (rmsd) of 0.636 Å for 151 common Cα atoms.

Expression of DmsB Mutants. Mutants of DmsABC were evaluated for their ability to support anaerobic growth in glycerol/Me_2SO minimal medium (Table 1). *E. coli* DSS301 cells (Δ*dmsABC*) transformed with plasmids encoding the DmsB-P80A, DmsB-D95A, DmsB-D97A, and DmsB-Y104A mutants exhibit shorter doubling times (3.0−4.2 h) than the wild-type enzyme (6.3 h), whereas cells transformed with plasmids encoding the DmsB-H85F, DmsB-H85T, DmsB-R103A, DmsB-H106A, and DmsB-H106E mutants have longer doubling times (8.5−12.4 h). The increased and decreased rates of growth of the aforementioned DmsB mutants can be correlated with the amount of DmsABC protein targeted to the membrane as determined by SDS−PAGE and immunoblotting (data not shown), as well as with the observed $BV^{+\bullet}$:Me_2SO specific enzyme activities (Table 1). Enzyme expression levels also agree with the FQ data on membranes prepared from *E. coli* HB101 (see below, Table 2); FQ titrations were not carried out for mutants expressed in DSS301 because of the high level of expression of fumarate reductase in this strain. Cells transformed with plasmids encoding the DmsB-P80H, DmsB-P80D, DmsB-S81G, DmsB-S81H, and DmsB-Y104D mutants are unable

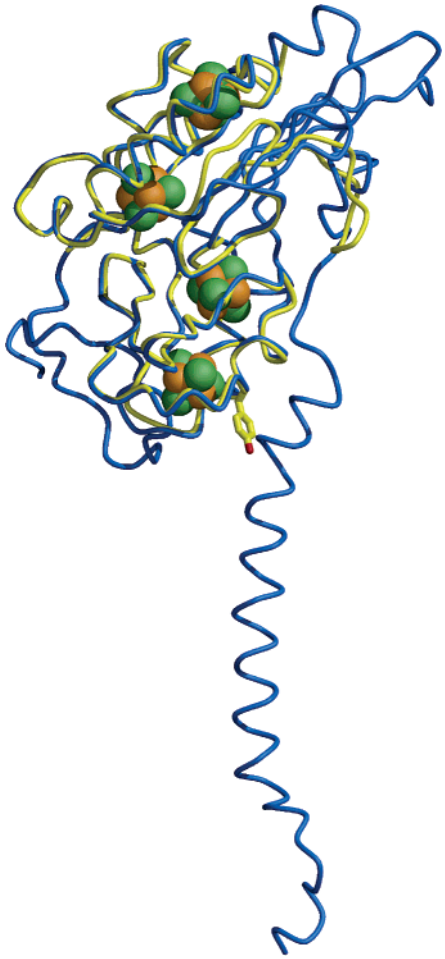

FIGURE 4: Three-dimensional alignment of the backbones of the DmsB model (yellow) and the structure of FdnH (blue). Using 151 common Cα atoms, a rmsd value of 0.636 was calculated from the superimposition of the two structures. Note that the FdnH subunit contains a C-terminal transmembrane tail which is absent in DmsB. An important residue, Y104 of DmsB, has its side chain shown in the figure.

to support anaerobic growth in glycerol/Me_2SO medium. DSS301 cells expressing the DmsB-Y104E mutant have a much longer doubling time (∼20 h) than DSS301 cells expressing the wild-type enzyme. For mutants that do not support growth, mutant enzymes are still observed in membrane preparations as detected by immunoblotting and the presence of $BV^{+\bullet}$:Me_3NO activities (data not shown).

Enzyme Activities of Wild-Type and Mutant DmsABC. Membrane preparations from *E. coli* DSS301 cells harboring the mutant plasmids were tested for their ability to accept electrons from either $BV^{+\bullet}$ or $LPCH_2$, and transfer them to Me_3NO (Table 1). The $BV^{+\bullet}$:Me_3NO assay detects whether DmsAB is assembled and is independent of a functional Q-site within DmsC, whereas the $LPCH_2$:Me_3NO assay requires a functional heterotrimer. A comparison of the $BV^{+\bullet}$:Me_3NO activity to the $LPCH_2$:Me_3NO activity can then be used to examine electron transfer from the Q-site to FS4 since such a ratio is independent of the amount of enzyme in the preparation and is therefore an intrinsic property of the DmsABC variant in question. In general, the levels of $BV^{+\bullet}$:Me_3NO specific activities correlate closely with the amount of mutant enzyme expressed in the cytoplasmic membrane, as determined by SDS−PAGE and immunoblotting (data not shown), as well as FQ titrations with

Table 1: Growth Rates of the DmsB Mutants in Glycerol/Me_2SO Minimal Media and the $BV^{+\bullet}$- and $LPCH_2$-Dependent Reduction of Me_3NO[a]

	doubling time (h)	$BV^{+\bullet}$:Me_3NO specific activity	$LPCH_2$:Me_3NO specific activity	$BV^{+\bullet}$:$LPCH_2$ activity ratio
wild type	6.3	35.4 ± 1.9	0.97 ± 0.01	36 ± 2
K77A	4.2	34.0 ± 0.0	1.10 ± 0.05	31 ± 1
P80A	3.0	115.9 ± 3.0	0.78 ± 0.03	149 ± 7
P80H	NG[b]	9.2 ± 0.2	0	N/A[c]
P80D	NG[b]	18.5 ± 0.1	0	N/A[c]
S81H	NG[b]	8.6 ± 0.1	0	N/A[c]
S81G	NG[b]	12.7 ± 0.4	0	N/A[c]
H85F	12.4	22.1 ± 0.5	0.69 ± 0.00	32 ± 1
H85T	11.7	24.1 ± 0.4	0.72 ± 0.02	34 ± 1
D95A	3.4	147.9 ± 5.3	5.56 ± 0.39	27 ± 2
D97A	3.6	166.6 ± 2.2	6.12 ± 0.25	27 ± 1
R103A	13.5	35.2 ± 1.9	0.81 ± 0.01	43 ± 2
Y104A	4.2	79.5 ± 4.6	0.86 ± 0.03	92 ± 6
Y104D	NG[b]	12.0 ± 0.8	0	N/A[c]
Y104E	~20	13.8 ± 0.8	0.32 ± 0.02	43 ± 4
H106A	11.4	14.4 ± 0.4	1.18 ± 0.02	12 ± 1
H106E	8.5	14.9 ± 0.2	0.43 ± 0.01	35 ± 1

[a] Mutant enzymes were expressed in *E. coli* DSS301 cells lacking a chromosomal copy of DMSO reductase. Enzyme specific activities are given in millimoles per minute per milligram of total protein with one standard deviation of error. [b] No growth. [c] Not applicable. The $BV^{+\bullet}$:$LPCH_2$ activity ratio cannot be determined because the $LPCH_2$:Me_3NO specific activity is zero.

Table 2: HOQNO FQ Titrations of DmsB Mutants Expressed in HB101 Cells[a]

	estimated K_d (nM)	[DmsABC] (nmol/mg of membrane protein)
wild type	5	0.60
K77A	5	0.57
P80A	10	0.74
P80D	17	0.60
P80H	20	0.48
S81G	20	0.24
S81H	20	0.24
H85F	5	0.38
H85T	5	0.26
D95A	5	0.88
D97A	5	1.16
C102S ([3Fe-4S])	5	0.57
C102W ([3Fe-4S])	17	0.27
R103A	5	0.42
Y104A	5	0.80
Y104D	10	0.63
Y104E	18	0.34
H106A	5	0.47

[a] The titration was repeated at three different protein concentrations and a best fit curve fitted to all three plots simultaneously to estimate the dissociation constants for HOQNO. Mutations of P80, S81, and Y104 of DmsB seem to have an effect on the affinity of the enzyme for HOQNO.

HOQNO (see below, Table 2). Comparison of the ratios of $BV^{+\bullet}$:Me_3NO activity to $LPCH_2$:Me_3NO activity indicates that the majority of DmsB mutants have ratios of approximately 35, which is equivalent to that of the wild-type enzyme. The DmsB-P80A and DmsB-Y104A mutants, however, have ratios of 149 and 92, respectively, which are dramatically higher than that of the wild-type enzyme. These two mutants also exhibit an altered K_m value for lapachol. The K_m values for $LPCH_2$ of the wild type, the DmsB-P80A mutant, and the DmsB-Y104A mutant are approximately 100, 47, and 210 μM, respectively. The corresponding k_{cat} values are approximately 64, 79, and 114 s^{-1}, respectively.

Table 3: Mutations Made in DmsB and the Resultant E_m Values of the [3Fe-4S] Cluster[a]

DmsB mutant	FS4 $E_{m,7}$ (mV)	significant $\Delta E_{m,7}$ (mV)
HB101/pDms160_C102S	275	−
K77A/C102S	260	−15
P80A/C102S	270	−
H85F/C102S	255	−20
H85T/C102S	260	−15
D95A/C102S	283	−
D95K/C102S	277	−
D97A/C102S	273	−
R103A/C102S	250	−25
Y104A/C102S	280	−
Y104D/C102S	150	−125
Y104E/C102S	145	−130
Y104D/H106F/C102S	130	−145
H106A/C102S	260	−15
H106I/C102S	250	−25
H106E/C102S	271	−

[a] Mutant enzymes were expressed in HB101 cells. The signal of the engineered FS4 was detected at a temperature of 12 K, a microwave power of 20 mW at 9.38 GHz, and a modulation amplitude of 10 G_{pp} at 100 kHz. The heights of the $g = 2.03$ peak of the [3Fe-4S] cluster in the oxidized state were plotted against the redox potentials in which the membranes were poised, and the Nernst equation was fitted to the data to determine $E_{m,7}$ values.

HOQNO FQ Titrations. HOQNO is a MQH_2 analogue inhibitor whose fluorescence in solution is quenched when it is bound to DmsABC (*51*). FQ titrations were carried out at three different enzyme concentrations to accurately estimate the affinity of the enzyme for HOQNO (K_d values) and the concentration of binding sites (Table 2). Mutations of K77, H85, D95, D97, R103, and H106 of DmsB do not affect the affinity of the enzyme for HOQNO (Table 2). However, P80, S81, and Y104 of DmsB appear to play an important role in defining the HOQNO binding site. The DmsB-P80A, DmsB-P80D, and DmsB-P80H mutations increase the K_d for HOQNO from 5 nM to 10, 17, and 20 nM, respectively; DmsB-S81G and DmsB-S81H mutations both increase the K_d to 20 nM. Interestingly, the DmsB-Y104A mutant has the same affinity for HOQNO as the wild-type enzyme; the DmsB-Y104D mutant increases the K_d to 10 nM, and the DmsB-Y104E mutant increases the K_d to 18 nM. The DmsB-C102S mutant does not affect HOQNO binding, but the DmsB-C102W mutant increases the K_d to 17 nM. These results support the assertion that the function of FS4 is closely coupled to that of a dissociable Q-site within the DmsC subunit (see the Discussion) (*12*).

Modulation of the [3Fe-4S] E_m Value. $FS4^{[4Fe-4S]}$ of DmsB can be converted to a [3Fe-4S] form ($FS4^{[3Fe-4S]}$) by mutagenesis of C102 of DmsB to a range of alternative residues (*4*). In a DmsB-C102S mutant, $FS4^{[3Fe-4S]}$ has an E_m of 275 mV compared to a value of −50 mV for $FS4^{[4Fe-4S]}$ of the wild-type enzyme (*12*). The high potential of $FS4^{[3Fe-4S]}$ renders its EPR spectrum free from overlapping signals arising from the other three [4Fe-4S] clusters of DmsB (FS1−FS3), and also from complications arising from spin−spin interactions with these centers. This greatly simplifies analyses of the effects that the DmsB mutants have on the EPR line shape and the E_m value. Double mutants were therefore made which contained the mutation of interest and the DmsB-C102S mutation. Potentiometric titrations of DmsB double mutants were performed, and the intensities

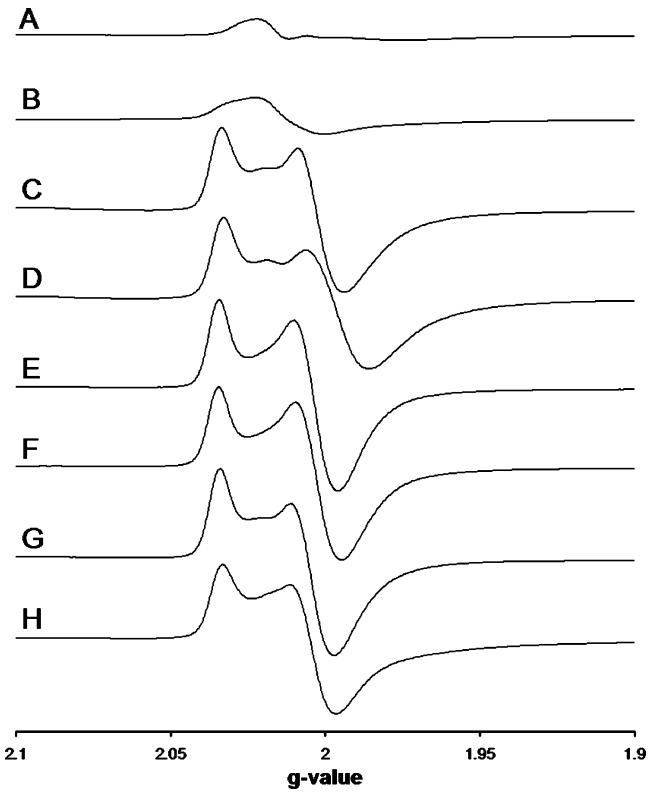

FIGURE 5: Oxidized EPR spectra of the engineered [3Fe-4S] cluster in DmsB in the absence and presence of HOQNO. When no DmsABC is expressed (A), or when only wild-type DmsABC is expressed (B), only the [3Fe-4S] cluster signal from fumarate reductase is observed. In the presence of 50 μM HOQNO, the peak-trough centered at $g = 2.00$ corresponding to $FS4^{[3Fe-4S]}$ of the DmsB-C102S mutant (C) is shifted upfield (D). In the DmsB-C102S/Y104D and DmsB-C102S/Y104E mutants, the EPR line shapes of the $FS4^{[3Fe-4S]}$ oxidized spectra are unchanged (E and G), and the upfield shift of the peak-trough is not observed in the presence of HOQNO (F and H).

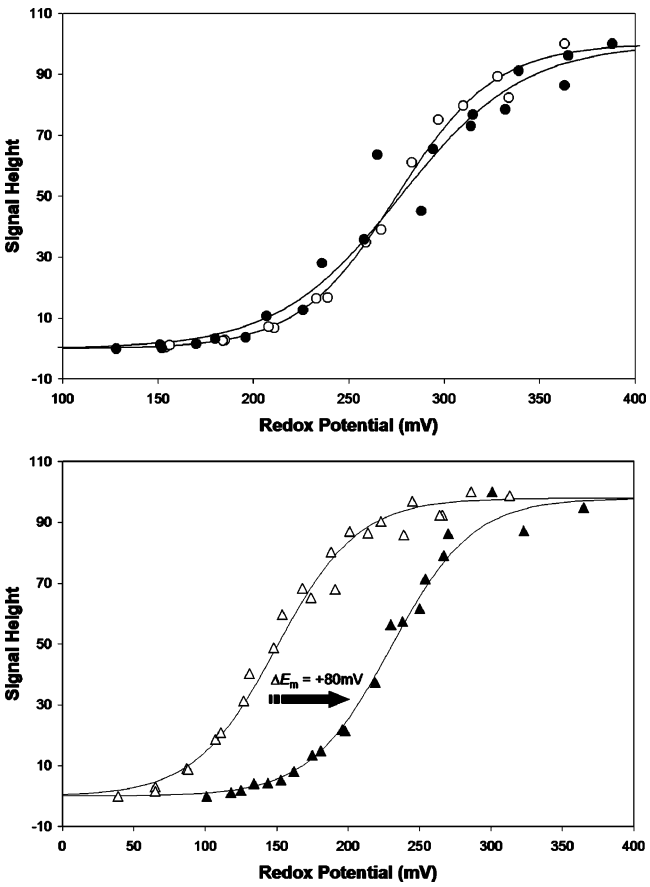

FIGURE 6: Redox titrations of FS4 from the DmsB-C102S single mutant (top) and the DmsB-C102S/Y104D mutant (bottom). In both the absence (○) and presence (●) of HOQNO, the E_m of the [3Fe-4S] cluster in the DmsB-C102S mutant is approximately 275 mV. For the DmsB-C102S/Y104D mutant, however, the E_m of the [3Fe-4S] cluster shifts from 150 mV in the absence (△) of HOQNO to 230 mV in the presence (▲) of HOQNO.

of the $g = 2.03$ peaks were plotted versus the ambient redox potential. The Nernst equation was used to fit the data points, and the resultant E_m values are listed in Table 3. $FS4^{[3Fe-4S]}$ of the DmsB-C102S mutant has an E_m of 275 mV, which agrees with the previously reported value (*4*). In general, mutations of positively charged residues to apolar and noncharged residues cause a small ΔE_m of approximately −15 to −25 mV for $FS4^{[3Fe-4S]}$. Mutations of acidic residues to alanine residues do not affect the $E_{m,7}$ of the [3Fe-4S] cluster. The DmsB-C102S/Y104E mutant causes a large ΔE_m from 275 to 145 mV. A similar mutant, DmsB-C102S/Y104D, also causes a large ΔE_m from 275 to 150 mV. Another mutant, DmsB-C102S/Y104E/H106F, exhibits an E_m of 130 mV for $FS4^{[3Fe-4S]}$.

Effects of HOQNO and pH on FS4. Expression of the mutants in *E. coli* TOPP2 reaches levels at which EPR spectra of oxidized inner membranes are dominated by the spectrum of $FS4^{[3Fe-4S]}$. Incubation of the oxidized DmsB-C102S mutant enzyme with HOQNO (5-fold molar excess) elicits a line shape change that is manifested by a shift in the position of the g_{xy} feature of the $FS4^{[3Fe-4S]}$ EPR spectrum (Figure 5C,D) (*12*). The DmsB-C102S/Y104D and DmsB-C102S/Y104E mutants have negligible effects on the EPR line shape of $FS4^{[3Fe-4S]}$ (Figure 5E,G). Although HOQNO binding is observed for these two mutants in FQ titrations (Table 2), it does not appear to elicit the expected change in their oxidized $FS4^{[3Fe-4S]}$ spectra (Figure 5F,H). Preliminary studies with a DmsB-Y104W mutant show that its g_{xy} feature of the $FS4^{[3Fe-4S]}$ spectrum can be shifted upfield in the presence of HOQNO despite this mutant having a lower affinity for the inhibitor (unpublished data). This suggests that an aromatic residue is essential for the observation of an HOQNO-induced EPR line shape change.

The potentiometric effect of acidic substitutions of Y104 of DmsB on the E_m of $FS4^{[3Fe-4S]}$ (a large $-\Delta E_m$) and the retention of high-affinity HOQNO binding prompted us to evaluate the potentiometric effects of inhibitor binding on the DmsB-C102S/Y104D mutant. In the presence of 50 μM HOQNO, the E_m of the DmsB-C102S single mutant remains unaltered ($E_m = 275$ mV). However, when a potentiometric titration is performed on the DmsB-C102S/Y104D mutant in the presence of HOQNO, the E_m of the $FS4^{[3Fe-4S]}$ cluster is increased from 150 to 230 mV (Figure 6). Given the inability of HOQNO to increase the E_m of $FS4^{[3Fe-4S]}$ in the DmsB-C102S mutant, we determined if a decrease in pH can bring about a corresponding increase in E_m in this particular mutant. In pH studies, the $E_{m,7}$, $E_{m,6}$, and $E_{m,5}$ of the DmsB-C102S mutant remain relatively unchanged at 275, 295, and 277 mV, respectively. Interestingly, if the $E_{m,7}$ of FS4 is lowered to 150 mV via the DmsB-C102S/Y104D mutation, the E_m of the cluster becomes dependent on pH

and $E_{m,6}$ and $E_{m,5}$ are approximately 165 and 200 mV, respectively.

DISCUSSION

By constructing and utilizing a model of DmsB based on the crystal structure of FdnH, we have identified the amino acids which are in the proximity of FS4, the [4Fe-4S] cluster closest to the membrane anchor subunit. This region of DmsABC is of interest because, unlike NarGHI and FdnGHI, DmsABC lacks heme in its membrane anchor subunit and the Q-site must communicate directly with FS4. To investigate the role of these amino acids, we examined the enzymatic activity, HOQNO binding, and redox properties of FS4 using a site-directed mutagenesis approach. We found that electron transfer from the MQH_2 binding site to the [Fe-S] clusters of DmsB is affected in the P80, S81, and Y104 mutants of DmsB. Q-Site and $FS4^{[3Fe-4S]}$ mutants of DmsABC do not affect the ability of DmsABC to accept electrons from $BV^{+\bullet}$ but hinder its ability to accept electrons from the MQH_2 analogue $LPCH_2$ (*4*, *12*, *13*). The ratio of $BV^{+\bullet}$:Me_3NO to $LPCH_2$:Me_3NO activities was not altered significantly in the DmsB-D95A and DmsB-D97A mutants, indicating the lack of an effect of these mutants on electron transfer from the Q-site to FS4. However, both $BV^{+\bullet}$:Me_3NO and $LPCH_2$:Me_3NO activities of these two mutants are higher than those of the wild-type enzyme by approximately 5-fold; this is caused, in part, by the stronger expression of the DmsB-D95A and DmsB-D97A mutants, as supported by the FQ data (Table 2) and immunoblotting (data not shown). Thus, the removal of an acidic residue near the DmsB−DmsC interface seems to allow either improved assembly of DmsABC or less degradation of DmsABC, as well as increasing the rate of electron flux through DmsB. Because the ratio of $BV^{+\bullet}$:Me_3NO to $LPCH_2$:Me_3NO activities is an intrinsic property of the enzyme and is independent of the amount of enzyme in a given preparation, the increased ratios for the DmsB-P80A and DmsB-Y104A mutants strongly indicate an impediment of electron transfer from the Q-site to FS4. To examine the redox properties of these mutations, we utilized a DmsB-C102S mutant that converts FS4 from a [4Fe-4S] cluster ($FS4^{[4Fe-4S]}$) to a [3Fe-4S] cluster ($FS4^{[3Fe-4S]}$) that is EPR-visible and magnetically isolated in its oxidized form. In the corresponding double mutants (DmsB-C102S/P80A and DmsB-C102S/Y104A), the E_m of the $FS4^{[3Fe-4S]}$ cluster remains unchanged at approximately 275 mV. Given that the E_m of $FS4^{[4Fe-4S]}$ remains unchanged in the single mutants, we surmise that the rate of electron transfer through the cofactors in DmsB is most likely unaffected in these mutants, but communication between the MQH_2 binding site and FS4 is disrupted.

The altered enzyme kinetics in the DmsB-P80A and DmsB-Y104A mutants suggest that these two residues play an important role in enzyme turnover. When the P80 residue of DmsB is changed to residues which have larger side chains, MQH_2 either is unable to bind or cannot be oxidized, and electrons are not transferred from the Q-site to FS4. This phenomenon also holds true for the DmsB-S81G, DmsB-S81H, DmsB-C102W, and DmsB-Y104D mutants. These mutants may distort the Q-site architecture by directly disrupting ligand interaction(s) or by indirectly altering the conformation of DmsC such that the Q-site is altered. Not only can distortions of the Q-site lead to lowered affinity of the enzyme for MQH_2, but they can also affect MQH_2 oxidation by displacing key residues involved in the catalytic cycle. This is not surprising since the three residues in FdnH corresponding to P80, S81, and Y104 of DmsB are located at the interface between the soluble dimer and the membrane anchor subunit in the FdnGHI structure (Figure 3) (*14*). In fact, the equivalent Tyr residue in FdnH directly interacts with the proximal heme of FdnI. The absence of heme in DmsC suggests that MQH_2 donates electrons directly to FS4 in a manner essentially identical to that seen in *E. coli* fumarate reductase where electrons are donated directly from the Q_p-site to the electron transfer subunit (*38*−*40*, *53*). The difference in HOQNO binding affinity between the DmsB-C102S (K_d = 5 nM) and DmsB-C102W (K_d = 17 nM) mutants implies that the Trp side chain sterically hinders a Q-site located in the DmsB−DmsC interface region. Examination of the NarGHI structure lends support to this suggestion (*17*); the indole side chain of W220 of NarH points toward the proximal heme (b_p) of NarI within the NarH−NarI interface region. In the crystal structure of SdhCDAB, the equivalent proline residue (P160 of SdhB) at the SdhB−SdhCD interface is shown to be one of two residues that "sandwiches" the bound UQ molecule (*54*). Furthermore, mutation of this proline residue in human Complex II results in an autosomal dominant disease called hereditary paraganglioma (*55*). Overall, given the FQ data presented herein and previously published data (*12*), we propose that the Q-site of DmsABC is in a location equivalent to those of FrdABCD and SdhCDAB.

Tyrosine residues have been implicated in the reaction scheme of many redox enzymes, including *E. coli* cytochrome bo_3 (*56*), yeast cytochrome bc_1 complex (*57*), cytochrome *c* oxidase (*58*, *59*), and photosystem II (*60*, *61*). The Y104 mutations of DmsB resulted in enzymes with quite different properties. The DmsB-Y104D mutant does not support growth in Me_2SO, whereas the DmsB-Y104E mutant is able to support growth but at a much slower rate. There is also a correlation between side chain length and the observed K_d for HOQNO with the DmsB-Y104D and DmsB-Y104E mutants. In contrast, the DmsB-Y104A mutant is able to support growth in Me_2SO and binds HOQNO with high affinity. Thus, DmsB-Y104 plays an integral role in defining Q-site function, and appears to be essential for both MQH_2 binding and oxidation. In the DmsB-Y104A mutant, it is likely that another residue is shifted into the position of the Y104 side chain and can complement its role in quinol oxidation and/or electron transfer. In the DmsB-Y104D mutant, the Asp residue is unable to perform the equivalent function. In the DmsB-Y104E mutant, however, the Glu carboxylate side chain is able to perform a function equivalent to that of a Tyr hydroxyl but at a lower efficiency, as indicated by the slower growth in minimal media and the low $LPCH_2$:Me_3NO activity. If Y104 functions as a proton acceptor in the mechanism of MQH_2 oxidation, then its hydroxyl group must be H-bonded or be positioned near a positively charged side chain so that its pK_a is lowered to allow protonation and/or deprotonation to readily occur at near-neutral pH values. Examination of the DmsB model and the FdnH structure reveals that no residues from DmsB can provide such a side chain to interact with Y104, suggesting that this modulating residue is most likely provided by DmsC.

Table 3 lists the mutations made in DmsB and their effects on the E_m of FS4. The most significant ΔE_m observed is from mutation of Y104 of DmsB to Asp and Glu, which lowers the E_m of the [3Fe-4S] cluster from 275 to 150 mV and from 275 to 145 mV, respectively. The DmsB-C102S/Y104D and DmsB-C102S/Y104E mutants both abolish the upfield shift of the peak-trough (g_{xy}) observed in their oxidized spectra in the presence of HOQNO (Figure 5), despite the observation of HOQNO binding in FQ titrations for the corresponding single mutants. This would suggest that an aromatic residue is essential for communication between the Q-site and FS4 and the HOQNO-dependent line shape change observed in the spectrum of $FS4^{[3Fe-4S]}$. Bulky aromatic residues have been suggested to play a role in modulating the E_m of [Fe-S] clusters (*32*, *62*), and the mutagenesis of Y104 of DmsB in this study clearly supports this view. However, Agarwal and co-workers found that a conserved Tyr in ferredoxins near a [4Fe-4S] cluster did not play a role in modulating the E_m of that cluster, but rather prevented solvent accessibility and cluster degradation (*63*).

The DmsB-C102S/P80A mutant does not alter the E_m of $FS4^{[3Fe-4S]}$. This observation is quite surprising, since backbone amide hydrogens are postulated to play a dominant role in modulating the E_m of [Fe-S] clusters through H-bonding interactions (*32*−*37*), and the DmsB-P80A mutation introduces an amide that points directly at FS4 based on the structures of FdnGHI and NarGHI (*14*, *17*). A plausible explanation for this is that the maximum allowable E_m for this particular [3Fe-4S] cluster may be approximately 275 mV. This rationale is supported by results from pH titrations as well as the effect of HOQNO binding on FS4. At pH 7, 6, and 5, the E_m values of the DmsB-C102S single mutant are independent of pH, whereas the DmsB-C102S/Y104D mutation causes the E_m of $FS4^{[3Fe-4S]}$ to increase with decreasing pH. $FS4^{[3Fe-4S]}$ in the DmsB-C102S mutant has an $E_{m,7}$ of 275 mV in the presence and absence of HOQNO, while in the DmsB-C102S/Y104D mutant, it has an $E_{m,7}$ of 230 mV in the presence of HOQNO and an $E_{m,7}$ of 150 mV in its absence. In addition, mutations of basic residues around FS4 cause the $E_{m,7}$ to decrease, while no increase in the $E_{m,7}$ is observed when acidic residues are mutated. The data strongly suggest that the maximum allowable E_m of Me_2SO reductase $FS4^{[3Fe-4S]}$ is approximately 275 mV. This contrasts with other systems in which [Fe-S] cluster E_m values can clearly exceed this value (*64*, *65*). Experiments to determine the reason for the apparent upper limit for the E_m value of $FS4^{[3Fe-4S]}$ are in progress.

The DmsB-C102S mutant is unable to support growth in glycerol/Me_2SO minimal medium, yet is clearly able to bind the MQH_2 analogue HOQNO. The endergonic rate-limiting step in electron transfer through both DMSO reductase and nitrate reductase is for electrons to travel from FS4 to FS2 (Figure 1). The $\Delta E_{m,7}$ for the FS4−FS2 pair is −600 mV in NarH, −280 mV in DmsB, −460 mV in the DmsB-C102S/Y104D/H106F mutant, and −605 mV in the DmsB-C102S mutant. The DmsB-C102S mutant is nonfunctional, although the $\Delta E_{m,7}$ for the FS4−FS2 pair is −605 mV, which is comparable to the value of −600 mV for NarH. One plausible explanation for this inconsistency lies in the E_m for nitrate reduction versus the reduction of Me_2SO. The E_m for nitrate reduction is much higher compared to the E_m of NarGHI FS4, but the E_m for Me_2SO reduction becomes smaller than the E_m of FS4 in the DmsB-C102S mutant, making it energetically unfavorable for the electron to travel from FS4 to the substrate. A second possibility lies in the fact that NarGHI possesses two heme moieties in the membrane-intrinsic domain which are lacking in DmsABC. Recently, a model by which electrons travel through NarGHI was proposed by our laboratory (*66*), whereby multiple electrons enter into heme b_d, heme b_p, and FS4 sequentially before the first electron surmounts the thermodynamically unfavorable FS4−FS2 energy hill. In this model, electrons from heme b_d and heme b_p can "push" an electron from FS4 to FS2. In DmsABC, however, this is impossible since it lacks heme in its membrane anchor subunit. Although the DmsB-C102S/Y104D and DmsB-C102S/Y104E mutants dramatically decrease the E_m of FS4, they are also unable to support growth on a glycerol/Me_2SO minimal medium. In light of our understanding that the Y104 residue in DmsB plays a role in the catalytic cycle of the enzyme, it is not surprising that these mutants are unable to perform their physiological function despite a large drop in the E_m of FS4.

In this study, a Tyr residue was discovered to play a major role in controlling the redox properties of an [Fe-S] cluster and for communication between an [Fe-S] cluster and the Q-site. Data obtained from other mutants created around this [Fe-S] cluster also indicate that positively charged residues may be responsible for fine-tuning the E_m of the [Fe-S] cluster by approximately 15−25 mV per charge. The DmsB-C102S/Y104D/H106F mutant shows that these two effects are additive in controlling the redox properties of the [Fe-S] cluster. By examining the structure of FdnGHI and the model of DmsABC, one can also surmise that certain charged residues may fine-tune the E_m of multiple redox centers during enzyme turnover. P80, S81, and Y104 of DmsB are located at the interface between the soluble dimer and the membrane anchor domain, and were shown to be important residues for MQH_2 binding and oxidation. These observations support a model for MQH_2 oxidation by DmsABC in which the Q-site donates electrons directly to FS4 (*12*). Such a model is very similar to that observed for FrdABCD in which the Q-site donates electrons directly to the [3Fe-4S] cluster (*39*, *40*).

Overall, the data presented herein illustrate the crucial role of FS4 as the first electron acceptor in the electron relay system defined by the four [4Fe-4S] clusters of DmsB. We have demonstrated that the high E_m value of this cluster in its [3Fe-4S] form is a significant barrier to electron transfer through DmsB, and that alterations in its immediate environment can have a significant effect on the Q-site of DmsC. A comparison of the constituent cofactors in DmsABC to those in NarGHI suggests a possible role of the heme in the latter enzyme to allow physiological electron transfer despite a large (−600 mV) endergonic step. These studies represent a significant step toward understanding the factors which regulate electron fluxes through [Fe-S] clusters in redox enzymes, and contribute to an emerging understanding of the thermodynamic barriers which govern electron transfer.

REFERENCES

1. Bilous, P. T., and Weiner, J. H. (1985) Dimethyl sulfoxide reductase activity by anaerobically grown *Escherichia coli* HB101, *J. Bacteriol. 162*, 1151−1155.

2. Sambasivarao, D., Scraba, D. G., Trieber, C., and Weiner, J. H. (1990) Organization of dimethyl sulfoxide reductase in the plasma membrane of *Escherichia coli*, *J. Bacteriol. 172*, 5938−5948.
3. Bilous, P. T., Cole, S. T., Anderson, W. F., and Weiner, J. H. (1988) Nucleotide sequence of the dmsABC operon encoding the anaerobic dimethylsulphoxide reductase of *Escherichia coli*, *Mol. Microbiol. 2*, 785−795.
4. Rothery, R. A., and Weiner, J. H. (1991) Alteration of the iron−sulfur cluster composition of *Escherichia coli* dimethyl sulfoxide reductase by site-directed mutagenesis, *Biochemistry 30*, 8296−8305.
5. Simala-Grant, J. L., and Weiner, J. H. (1996) Kinetic analysis and substrate specificity of *Escherichia coli* dimethyl sulfoxide reductase, *Microbiology 142* (Part 11), 3231−3239.
6. Weiner, J. H., Rothery, R. A., Sambasivarao, D., and Trieber, C. A. (1992) Molecular analysis of dimethylsulfoxide reductase: A complex iron−sulfur molybdoenzyme of *Escherichia coli*, *Biochim. Biophys. Acta 1102*, 1−18.
7. Sambasivarao, D., Turner, R. J., Simala-Grant, J. L., Shaw, G., Hu, J., and Weiner, J. H. (2000) Multiple roles for the twin arginine leader sequence of dimethyl sulfoxide reductase of *Escherichia coli*, *J. Biol. Chem. 275*, 22526−22531.
8. Rothery, R. A., Grant, J. L., Johnson, J. L., Rajagopalan, K. V., and Weiner, J. H. (1995) Association of molybdopterin guanine dinucleotide with *Escherichia coli* dimethyl sulfoxide reductase: Effect of tungstate and a mob mutation, *J. Bacteriol. 177*, 2057−2063.
9. Cammack, R., and Weiner, J. H. (1990) Electron paramagnetic resonance spectroscopic characterization of dimethyl sulfoxide reductase of *Escherichia coli*, *Biochemistry 29*, 8410−8416.
10. Weiner, J. H., Shaw, G., Turner, R. J., and Trieber, C. A. (1993) The topology of the anchor subunit of dimethyl sulfoxide reductase of *Escherichia coli*, *J. Biol. Chem. 268*, 3238−3244.
11. Sambasivarao, D., and Weiner, J. H. (1991) Dimethyl sulfoxide reductase of *Escherichia coli*: An investigation of function and assembly by use of in vivo complementation, *J. Bacteriol. 173*, 5935−5943.
12. Rothery, R. A., and Weiner, J. H. (1996) Interaction of an engineered [3Fe-4S] cluster with a menaquinol binding site of *Escherichia coli* DMSO reductase, *Biochemistry 35*, 3247−3257.
13. Geijer, P., and Weiner, J. H. (2004) Glutamate 87 is important for menaquinol binding in DmsC of the DMSO reductase (DmsABC) from *Escherichia coli*, *Biochim. Biophys. Acta 1660*, 66−74.
14. Jormakka, M., Tornroth, S., Byrne, B., and Iwata, S. (2002) Molecular basis of proton motive force generation: Structure of formate dehydrogenase-N, *Science 295*, 1863−1868.
15. Berg, B. L., Li, J., Heider, J., and Stewart, V. (1991) Nitrate-inducible formate dehydrogenase in *Escherichia coli* K-12. I. Nucleotide sequence of the fdnGHI operon and evidence that opal (UGA) encodes selenocysteine, *J. Biol. Chem. 266*, 22380−22385.
16. Abaibou, H., Pommier, J., Benoit, S., Giordano, G., and Mandrand-Berthelot, M. A. (1995) Expression and characterization of the *Escherichia coli* fdo locus and a possible physiological role for aerobic formate dehydrogenase, *J. Bacteriol. 177*, 7141−7149.
17. Bertero, M. G., Rothery, R. A., Palak, M., Hou, C., Lim, D., Blasco, F., Weiner, J. H., and Strynadka, N. C. (2003) Insights into the respiratory electron transfer pathway from the structure of nitrate reductase A, *Nat. Struct. Biol. 10*, 681−687.
18. Blasco, F., Guigliarelli, B., Magalon, A., Asso, M., Giordano, G., and Rothery, R. A. (2001) The coordination and function of the redox centres of the membrane-bound nitrate reductases, *Cell. Mol. Life Sci. 58*, 179−193.
19. Rothery, R. A., Bertero, M. G., Cammack, R., Palak, M., Blasco, F., Strynadka, N. C., and Weiner, J. H. (2004) The catalytic subunit of *Escherichia coli* nitrate reductase A contains a novel [4Fe-4S] cluster with a high-spin ground state, *Biochemistry 43*, 5324−5333.
20. Heinzinger, N. K., Fujimoto, S. Y., Clark, M. A., Moreno, M. S., and Barrett, E. L. (1995) Sequence analysis of the phs operon in *Salmonella typhimurium* and the contribution of thiosulfate reduction to anaerobic energy metabolism, *J. Bacteriol. 177*, 2813−2820.
21. Krafft, T., Bokranz, M., Klimmek, O., Schroder, I., Fahrenholz, F., Kojro, E., and Kroger, A. (1992) Cloning and nucleotide sequence of the psrA gene of *Wolinella succinogenes* polysulphide reductase, *Eur. J. Biochem. 206*, 503−510.
22. Dietrich, W., and Klimmek, O. (2002) The function of methylmenaquinone-6 and polysulfide reductase membrane anchor (PsrC) in polysulfide respiration of *Wolinella succinogenes*, *Eur. J. Biochem. 269*, 1086−1095.
23. Guigliarelli, B., Magalon, A., Asso, M., Bertrand, P., Frixon, C., Giordano, G., and Blasco, F. (1996) Complete coordination of the four Fe−S centers of the β subunit from *Escherichia coli* nitrate reductase. Physiological, biochemical, and EPR characterization of site-directed mutants lacking the highest or lowest potential [4Fe-4S] clusters, *Biochemistry 35*, 4828−4836.
24. Rothery, R. A., Magalon, A., Giordano, G., Guigliarelli, B., Blasco, F., and Weiner, J. H. (1998) The molybdenum cofactor of *Escherichia coli* nitrate reductase A (NarGHI). Effect of a mobAB mutation and interactions with [Fe−S] clusters, *J. Biol. Chem. 273*, 7462−7469.
25. Manodori, A., Cecchini, G., Schroder, I., Gunsalus, R. P., Werth, M. T., and Johnson, M. K. (1992) [3Fe-4S] to [4Fe-4S] cluster conversion in *Escherichia coli* fumarate reductase by site-directed mutagenesis, *Biochemistry 31*, 2703−2712.
26. Kowal, A. T., Werth, M. T., Manodori, A., Cecchini, G., Schroder, I., Gunsalus, R. P., and Johnson, M. K. (1995) Effect of cysteine to serine mutations on the properties of the [4Fe-4S] center in *Escherichia coli* fumarate reductase, *Biochemistry 34*, 12284−12293.
27. Condon, C., Cammack, R., Patil, D. S., and Owen, P. (1985) The succinate dehydrogenase of *Escherichia coli*. Immunochemical resolution and biophysical characterization of a 4-subunit enzyme complex, *J. Biol. Chem. 260*, 9427−9434.
28. Unciuleac, M., Warkentin, E., Page, C. C., Boll, M., and Ermler, U. (2004) Structure of a xanthine oxidase-related 4-hydroxybenzoyl-CoA reductase with an additional [4Fe-4S] cluster and an inverted electron flow, *Structure 12*, 2249−2256.
29. Page, C. C., Moser, C. C., Chen, X., and Dutton, P. L. (1999) Natural engineering principles of electron tunnelling in biological oxidation−reduction, *Nature 402*, 47−52.
30. Page, C. C., Moser, C. C., and Dutton, P. L. (2003) Mechanism for electron transfer within and between proteins, *Curr. Opin. Chem. Biol. 7*, 551−556.
31. Stephens, P. J., Jollie, D. R., and Warshel, A. (1996) Protein Control of Redox Potentials of Iron−Sulfur Proteins, *Chem. Rev. 96*, 2491−2514.
32. Chen, K., Bonagura, C. A., Tilley, G. J., McEvoy, J. P., Jung, Y. S., Armstrong, F. A., Stout, C. D., and Burgess, B. K. (2002) Crystal structures of ferredoxin variants exhibiting large changes in [Fe−S] reduction potential, *Nat. Struct. Biol. 9*, 188−192.
33. Langen, R., Jensen, G. M., Jacob, U., Stephens, P. J., and Warshel, A. (1992) Protein control of iron−sulfur cluster redox potentials, *J. Biol. Chem. 267*, 25625−25627.
34. Jensen, G. M., Warshel, A., and Stephens, P. J. (1994) Calculation of the redox potentials of iron−sulfur proteins: The 2-/3-couple of [Fe4S*4Cys4] clusters in *Peptococcus aerogenes* ferredoxin, *Azotobacter vinelandii* ferredoxin I, and *Chromatium vinosum* high-potential iron protein, *Biochemistry 33*, 10911−10924.
35. Adman, E., Watenpaugh, K. D., and Jensen, L. H. (1975) NH−S hydrogen bonds in *Peptococcus aerogenes* ferredoxin, *Clostridium pasteurianum* rubredoxin, and *Chromatium* high potential iron protein, *Proc. Natl. Acad. Sci. U.S.A. 72*, 4854−4858.
36. Rayment, I., Wesenberg, G., Meyer, T. E., Cusanovich, M. A., and Holden, H. M. (1992) Three-dimensional structure of the high-potential iron−sulfur protein isolated from the purple phototrophic bacterium *Rhodocyclus tenuis* determined and refined at 1.5 Å resolution, *J. Mol. Biol. 228*, 672−686.
37. Jang, S. B., Seefeldt, L. C., and Peters, J. W. (2000) Modulating the midpoint potential of the [4Fe-4S] cluster of the nitrogenase Fe protein, *Biochemistry 39*, 641−648.
38. Rothery, R. A., and Weiner, J. H. (1998) Interaction of a menaquinol binding site with the [3Fe-4S] cluster of *Escherichia coli* fumarate reductase, *Eur. J. Biochem. 254*, 588−595.
39. Iverson, T. M., Luna-Chavez, C., Cecchini, G., and Rees, D. C. (1999) Structure of the *Escherichia coli* fumarate reductase respiratory complex, *Science 284*, 1961−1966.
40. Cecchini, G., Schroder, I., Gunsalus, R. P., and Maklashina, E. (2002) Succinate dehydrogenase and fumarate reductase from *Escherichia coli*, *Biochim. Biophys. Acta 1553*, 140−157.
41. Hagerhall, C. (1997) Succinate:quinone oxidoreductases. Variations on a conserved theme, *Biochim. Biophys. Acta 1320*, 107−141.
42. Altschul, S. F., Madden, T. L., Schaffer, A. A., Zhang, J., Zhang, Z., Miller, W., and Lipman, D. J. (1997) Gapped BLAST and PSI-BLAST: A new generation of protein database search programs, *Nucleic Acids Res. 25*, 3389−3402.

43. Fiser, A., and Sali, A. (2003) Modeller: Generation and refinement of homology-based protein structure models, *Methods Enzymol. 374*, 461−491.
44. Laskowski, R. A., MacAuthur, M. W., Moss, D. S., and Thorton, J. M. (1993) *J. Appl. Crystallogr. 26*, 283−291.
45. Rothery, R. A., Trieber, C. A., and Weiner, J. H. (1999) Interactions between the molybdenum cofactor and iron−sulfur clusters of *Escherichia coli* dimethylsulfoxide reductase, *J. Biol. Chem. 274*, 13002−13009.
46. Sambrook, J., and Russell, D. W. (2001) *Molecular cloning: A laboratory manual*, 3rd ed., Cold Spring Harbor Laboratory Press, Plainview, NY.
47. Markwell, M. A., Haas, S. M., Bieber, L. L., and Tolbert, N. E. (1978) A modification of the Lowry procedure to simplify protein determination in membrane and lipoprotein samples, *Anal. Biochem. 87*, 206−210.
48. Rothery, R. A., Chatterjee, I., Kiema, G., McDermott, M. T., and Weiner, J. H. (1998) Hydroxylated naphthoquinones as substrates for *Escherichia coli* anaerobic reductases, *Biochem. J. 332* (Part 1), 35−41.
49. Van Ark, G., and Berden, J. A. (1977) Binding of HQNO to beef-heart sub-mitochondrial particles, *Biochim. Biophys. Acta 459*, 119−127.
50. Okun, J. G., Lummen, P., and Brandt, U. (1999) Three classes of inhibitors share a common binding domain in mitochondrial complex I (NADH:ubiquinone oxidoreductase), *J. Biol. Chem. 274*, 2625−2630.
51. Zhao, Z., and Weiner, J. H. (1998) Interaction of 2-*n*-heptyl-4-hydroxyquinoline-*N*-oxide with dimethyl sulfoxide reductase of *Escherichia coli*, *J. Biol. Chem. 273*, 20758−20763.
52. Berks, B. C., Page, M. D., Richardson, D. J., Reilly, A., Cavill, A., Outen, F., and Ferguson, S. J. (1995) Sequence analysis of subunits of the membrane-bound nitrate reductase from a denitrifying bacterium: The integral membrane subunit provides a prototype for the dihaem electron-carrying arm of a redox loop, *Mol. Microbiol. 15*, 319−331.
53. Iverson, T. M., Luna-Chavez, C., Croal, L. R., Cecchini, G., and Rees, D. C. (2002) Crystallographic studies of the *Escherichia coli* quinol-fumarate reductase with inhibitors bound to the quinol-binding site, *J. Biol. Chem. 277*, 16124−16130.
54. Yankovskaya, V., Horsefield, R., Tornroth, S., Luna-Chavez, C., Miyoshi, H., Leger, C., Byrne, B., Cecchini, G., and Iwata, S. (2003) Architecture of succinate dehydrogenase and reactive oxygen species generation, *Science 299*, 700−704.
55. Astuti, D., Latif, F., Dallol, A., Dahia, P. L., Douglas, F., George, E., Skoldberg, F., Husebye, E. S., Eng, C., and Maher, E. R. (2001) Gene mutations in the succinate dehydrogenase subunit SDHB cause susceptibility to familial pheochromocytoma and to familial paraganglioma, *Am. J. Hum. Genet. 69*, 49−54.
56. Wang, J., Rumbley, J., Ching, Y. C., Takahashi, S., Gennis, R. B., and Rousseau, D. L. (1995) Reaction of cytochrome bo_3 with oxygen: Extra redox center(s) are present in the protein, *Biochemistry 34*, 15504−15511.
57. Wang, Y., and Beattie, D. S. (2002) Molecular modeling studies of the DCCD-treated cytochrome bc_1 complex: Predicted conformational changes and inhibition of proton translocation, *J. Bioenerg. Biomembr. 34*, 81−88.
58. Ostermeier, C., Harrenga, A., Ermler, U., and Michel, H. (1997) Structure at 2.7 Å resolution of the *Paracoccus denitrificans* two-subunit cytochrome *c* oxidase complexed with an antibody FV fragment, *Proc. Natl. Acad. Sci. U.S.A. 94*, 10547−10553.
59. Yoshikawa, S., Shinzawa-Itoh, K., Nakashima, R., Yaono, R., Yamashita, E., Inoue, N., Yao, M., Fei, M. J., Libeu, C. P., Mizushima, T., Yamaguchi, H., Tomizaki, T., and Tsukihara, T. (1998) Redox-coupled crystal structural changes in bovine heart cytochrome *c* oxidase, *Science 280*, 1723−1729.
60. Barry, B. A., and Babcock, G. T. (1987) Tyrosine radicals are involved in the photosynthetic oxygen-evolving system, *Proc. Natl. Acad. Sci. U.S.A. 84*, 7099−7103.
61. Babcock, G. T., Barry, B. A., Debus, R. J., Hoganson, C. W., Atamian, M., McIntosh, L., Sithole, I., and Yocum, C. F. (1989) Water oxidation in photosystem II: From radical chemistry to multielectron chemistry, *Biochemistry 28*, 9557−9565.
62. Ryle, M. J., Lanzilotta, W. N., and Seefeldt, L. C. (1996) Elucidating the mechanism of nucleotide-dependent changes in the redox potential of the [4Fe-4S] cluster in nitrogenase iron protein: The role of phenylalanine 135, *Biochemistry 35*, 9424−9434.
63. Agarwal, A., Li, D., and Cowan, J. A. (1995) Role of aromatic residues in stabilization of the [Fe4S4] cluster in high-potential iron proteins (HiPIPs): Physical characterization and stability studies of Tyr-19 mutants of *Chromatium vinosum* HiPIP, *Proc. Natl. Acad. Sci. U.S.A. 92*, 9440−9444.
64. Heering, H. A., Bulsink, B. M., Hagen, W. R., and Meyer, T. E. (1995) Influence of charge and polarity on the redox potentials of high-potential iron−sulfur proteins: Evidence for the existence of two groups, *Biochemistry 34*, 14675−14686.
65. Ambler, R. P., Daniel, M., Meyer, T. E., and Cusanovich, M. A. (1999) Amino acid sequences of two high-potential iron−sulfur proteins (HiPIPs) from the moderately halophilic purple phototrophic bacterium, *Rhodospirillum salinarum*, *Arch. Biochem. Biophys. 369*, 143−148.
66. Zhao, Z., Rothery, R. A., and Weiner, J. H. (2003) Transient kinetic studies of heme reduction in *Escherichia coli* nitrate reductase A (NarGHI) by menaquinol, *Biochemistry 42*, 5403−5413.

BI050362P